Acta Pharmaceutica Sinica B 2021;11(11):3665−3677

Chinese Pharmaceutical Association
Institute of Materia Medica, Chinese Academy of Medical Sciences

Acta Pharmaceutica Sinica B

www.elsevier.com/locate/apsb
www.sciencedirect.com

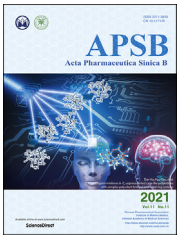

ORIGINAL ARTICLE

Spatial-resolved metabolomics reveals tissue-specific metabolic reprogramming in diabetic nephropathy by using mass spectrometry imaging

Zhonghua Wang[a,b,e,†], Wenqing Fu[a,b,†], Meiling Huo[a,b], Bingshu He[b], Yaqi Liu[b], Lu Tian[c], Wanfang Li[c], Zhi Zhou[a,b], Baili Wang[d], Jianzhen Xia[d], Yanhua Chen[a,b], Jinfeng Wei[c], Zeper Abliz[a,b,e,*]

[a]*Key Laboratory of Mass Spectrometry Imaging and Metabolomics (Minzu University of China), National Ethnic Affairs Commission, Beijing 100081, China*
[b]*College of Life and Environmental Sciences, Minzu University of China, Beijing 100081, China*
[c]*New Drug Safety Evaluation Center, Institute of Materia Medica, Peking Union Medical College, Beijing 100050, China*
[d]*School Hospital, Minzu University of China, Beijing 100081, China*
[e]*Key Laboratory of Ethnomedicine of Ministry of Education, School of Pharmacy, Minzu University of China, Beijing 100081, China*

Received 26 February 2021; received in revised form 26 April 2021; accepted 5 May 2021

Abbreviations: ADP, adenosine diphosphate; AFADESI, air flow-assisted desorption electrospray ionization; AGEs, advanced glycation end products; AMP, adenosine monophosphate; AMPK, adenosine monophosphate activated protein kinase; AST, astragaloside IV; ATP, adenosine triphosphate; BUN, blood urea nitrogen; CL, cardiolipin; Cre, creatinine; DAG, diacylglycerol; DESI, desorption electrospray ionization; DM, diabetes mellitus; DN, diabetic nephropathy; DPA, docosapentaenoic acid; ESKD, end-stage kidney disease; FBG, fasting blood glucose; GLU, glucose; HbA1c, glycosylated hemoglobin; GMP, guanosine monophosphate; GSH, glutathione; H&E, hematoxylin and eosin; HPLC, high-performance liquid chromatography; LysoPC, lysophosphatidylcholine; LysoPG, lysophosphatidylglycerol; MALDI, matrix-assisted laser desorption ionization; MS, mass spectrometry; MSI, mass spectrometry imaging; Na-CMC, sodium carboxymethyl cellulose; NMR, nuclear magnetic resonance; p-AMPK, phosphorylated adenosine monophosphate activated protein kinase; PA, phosphatidic acid; PC, phosphatidylcholine; PE, phosphatidylethanolamine; PG, phosphatidylglycerol; PPP, pentose phosphate pathway; PS, phosphatidylserine; PUFA, polyunsaturated fatty acids; ROI, regions of interest; ROS, reactive oxygen species; SDH, succinate dehydrogenase; SGLTs, sodium-glucose cotransporters; SM, sphingomyelin; STZ, streptozotocin; TCHO, total cholesterol; TCA, tricarboxylic acid; TG, triglyceride; UMP, uridine monophosphate; VIP, variable importance in projection.

*Corresponding author. Tel./fax: +86 10 68932646.
E-mail address: zeper@muc.edu.cn (Zeper Abliz).

†These authors made equal contributions to this work.

Peer review under responsibility of Chinese Pharmaceutical Association and Institute of Materia Medica, Chinese Academy of Medical Sciences.

https://doi.org/10.1016/j.apsb.2021.05.013

KEY WORDS

Spatial-resolved metabolomics;
Mass spectrometry imaging;
Diabetic nephropathy;
Metabolic reprogramming;
Astragaloside IV

Abstract Detailed knowledge on tissue-specific metabolic reprogramming in diabetic nephropathy (DN) is vital for more accurate understanding the molecular pathological signature and developing novel therapeutic strategies. In the present study, a spatial-resolved metabolomics approach based on air flow-assisted desorption electrospray ionization (AFADESI) and matrix-assisted laser desorption ionization (MALDI) integrated mass spectrometry imaging (MSI) was proposed to investigate tissue-specific metabolic alterations in the kidneys of high-fat diet-fed and streptozotocin (STZ)-treated DN rats and the therapeutic effect of astragaloside IV, a potential anti-diabetic drug, against DN. As a result, a wide range of functional metabolites including sugars, amino acids, nucleotides and their derivatives, fatty acids, phospholipids, sphingolipids, glycerides, carnitine and its derivatives, vitamins, peptides, and metal ions associated with DN were identified and their unique distribution patterns in the rat kidney were visualized with high chemical specificity and high spatial resolution. These region-specific metabolic disturbances were ameliorated by repeated oral administration of astragaloside IV (100 mg/kg) for 12 weeks. This study provided more comprehensive and detailed information about the tissue-specific metabolic reprogramming and molecular pathological signature in the kidney of diabetic rats. These findings highlighted the promising potential of AFADESI and MALDI integrated MSI based metabolomics approach for application in metabolic kidney diseases.

1. Introduction

As a major complication of diabetes mellitus (DM), diabetic nephropathy (DN) has become the leading cause of end-stage kidney disease (ESKD), posing a serious threat to human health with an increasing incidence worldwide[1–5] Extensive studies have been conducted to investigate the pathogenesis of DN, revealing that its occurrence and development involve the interaction of multiple factors and multiple metabolic pathways, such as genetic factors, abnormal renal hemodynamics, metabolic abnormalities caused by hyperglycemia, oxidative stress induced by increased advanced glycation end product generation, apoptosis, and inflammation[6–10]. However, detailed metabolic mechanisms underlying the pathogenesis of DN remain unknown.

Metabolic profiling of functional metabolites with spatial distribution in biosamples will provide important *in situ* biochemical information for tissue-specific molecular histology and pathology, which is key for more accurately understanding the molecular mechanism underlying diseases. Although high-performance liquid chromatography–mass spectrometry (HPLC–MS) and nuclear magnetic resonance (NMR) based metabolomics studies have greatly enhanced our understanding on diabetic kidney disease[11–14], little information regarding the spatial distribution of metabolites in diabetic kidney can be obtained through the analysis of homogeneous biological samples, such as urine, serum, and renal tissue homogenate, using HPLC–MS and NMR.

Mass spectrometry imaging (MSI) is a powerful molecular imaging technique that can be used *in situ* analysis of multiple known and unknown metabolites simultaneously[15,16], providing spatially resolved chemical information. Matrix-assisted laser desorption ionization (MALDI)-MSI is one of the most widely used MSI technologies in the field of biomedical research[17,18]. Generally, the imaging of molecules using MALDI-MSI is highly matrix-dependent. It remains challenging to detect a broad range of low-molecular-weight metabolites using MALDI-MSI because of the interference of matrix peaks[19]. However, high-sensitivity and spatial resolution imaging of certain types of metabolites can be achieved *via* MALDI-MSI using an appropriate matrix and optimized matrix deposition procedure[20]. Recently, ambient molecular imaging technique initiated by desorption electrospray ionization (DESI)-MSI has emerged as a promising tool for "direct" detection of small molecular in tissue sections because it can function without tedious matrix deposition processes[17]. In addition, ambient air-flow-assisted desorption electrospray ionization (AFADESI)-MSI can reportedly visualize thousands of structure-specific and functionally relevant metabolites in an untargeted analysis[21], thus showing good application prospect in high-throughput molecular pathology analysis. The spatial resolution of DESI-MSI and AFADESI-MSI is approximately 100 μm, which is lower than that of MALDI-MSI. A few MALDI-MSI and DESI-MSI methods have been used to separately visualize metabolic changes in renal sections of DN animal models[22,23]. However, the range of measurable metabolites and spatial resolution of MS imaging is limited, restricting their ability to provide a comprehensive insight into the metabolic reprogramming in diabetic kidneys.

In the present study, a spatial-resolved metabolic profiling approach based on AFADESI- and MALDI-MSI was proposed in order to obtain more complete and detailed information about region-specific metabolic reprogramming during DN development. Positive and negative AFADESI-MSI was used to identify and visualize the global metabolic alteration in the kidney of a high-fat diet-fed and streptozotocin (STZ)-treated DN model, and then the precise location of the discriminating metabolites in renal cortex was mapped by high-spatial-resolution MALDI-MSI. In addition, the metabolic impact of astragaloside IV (AST), a potential anti-diabetic drug, on DN, was also investigated by AFADESI-MSI. The proposed research strategy is shown in Fig. 1.

2. Materials and methods

2.1. Chemicals and reagents

HPLC-grade acetonitrile and methanol were purchased from Merck (Muskegon, MI, USA). AST was purchased from Chengdu ConBon Biotech Co., Ltd. (Chengdu, China). 1,5-Diaminonaphthalene (1,5-

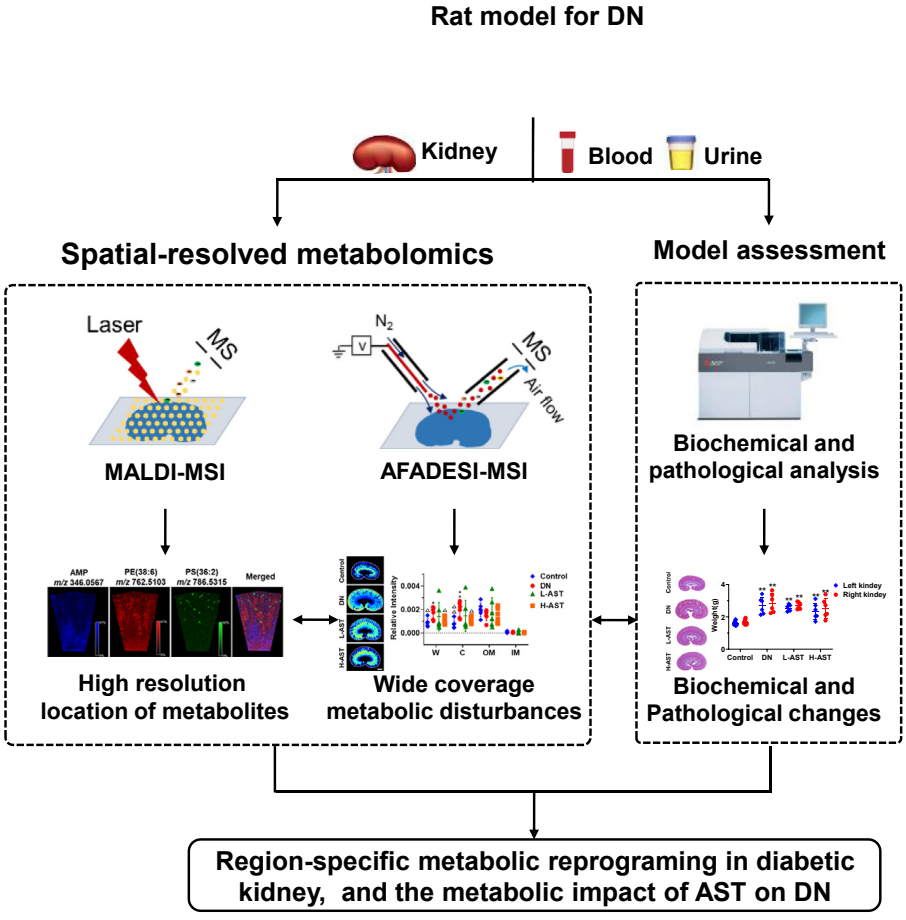

Figure 1 Research scheme for spatial-resolved metabolic reprogramming in diabetic nephropathy (DN) using air-flow-assisted desorption electrospray ionization (AFADESI) and matrix-assisted laser desorption ionization (MALDI) integrated mass spectrometry imaging (MSI).

DAN), STZ, citrate, and sodium carboxymethyl cellulose (Na-CMC) were purchased from Sigma−Aldrich (St. Louis, MO, USA).

2.2. *Animal model*

Six-week-old male WISTAR rats (180−200 g) were purchased from Vital River Laboratory Animal Technology Co., Ltd. (Beijing, China). The rats were randomized to the control (n = 6) and model groups (n = 32) and fed a normal pellet diet and high-fat diet, respectively, for 4 weeks. Then, model rats were injected intraperitoneally (ip) with a low dose of STZ (35 mg/kg), whereas control rats were administered citrate buffer (pH 4.4, vehicle) in a dose volume of 1 mL/kg, i.p. Five to seven days after STZ or vehicle injection, the fasting blood glucose (FBG) level was measured. Model rats with the FBG levels of ≥16.7 mmol/L for 3 consecutive days were considered diabetic and selected for further pharmacological studies. The diabetic rats were then randomized to the DN (n = 6), low-dose AST (L-AST, n = 6) group, and high-dose treated AST groups (H-AST, n = 6). Rats in the L-AST and H-AST groups were administered AST at an intragastric doses of 20 and 100 mg/kg (once daily), respectively. The control and DN group rats were treated with 0.5% Na-CMC (vehicle). During treatment, water consumption, food consumption, and body weight were monitored weekly, and FBG levels were measured every 2 weeks. After 12 weeks of treatment, 24-h urine samples were collected from each rat using metabolic cages. Blood samples were collected from the abdominal artery, and the kidneys were harvested, weighed, and snap-frozen in liquid nitrogen. All samples were stored at −80 °C until analysis. The animal experiments were conducted in accordance with the NIH Guide for the Care and Use of Laboratory Animals (National Institutes of Health Publication, No. 3040-2, revised 1999, Bethesda, MD, USA) and were approved by animal welfare ethics committee of Beijing Union-Genius Pharmaceutical Technology Development Co., Ltd. (Beijing, China).

2.3. *Biochemical analysis and hematoxylin eosin (H&E) staining*

FBG levels were measured using a blood glucose meter (Roche, Basel, Switzerland). Glycosylated hemoglobin (HbA1c) concentrations were measured using a Quo-Test HbA1c Analyzer (QUOTIENT Diagnostics Ltd. Walton-on-Thames, Surrey, UK).

The blood biochemical parameters including urea nitrogen, creatinine, uric acid, total cholesterol, glucose, and triglyceride levels were determined using an AU480 automatic chemistry analyzer (Beckman Coulter Inc., Brea, CA, USA). Urinary creatinine, K^+, Na^+, Cl^-, and Ca^{2+} concentrations were also determined using the AU480 automatic chemistry analyzer.

Frozen renal sections (10 μm) were prepared on a CM1860 cryostat (Leica Microsystems Ltd., Wetzlar, Germany) at −18 °C and mounted onto adhesion microscope slides. The H&E staining

was used to examine the histopathological lesions of renal sections.

2.4. AFADESI- and MALDI-MSI analysis of renal sections

AFADESI-MSI was performed on a lab-built AFADESI-MSI platform consisting of an AFADESI ambient ion source and a Q-OT-qIT hybrid mass spectrometer (Orbitrap Fusion Lumos; Thermo Fisher Scientific, San Jose, CA, USA). The mass spectra were acquired in a positive and negative full MS mode with a scan range of 100−1000 Da, mass resolution of 120,000 at m/z 200. More details were provided in Supporting Information and can be referred to our previously reported works[21,24].

For MALDI-MSI analysis, an automatic TM-Sprayer™ tissue imaging matrix sprayer (HTX Technologies, Carrboro, NC, USA) was used to achieve a matrix/analyte co-crystal size of less than 20 μm to support the imaging of metabolites at spatial resolutions of 20 and 200 μm. The matrix solution of 1,5-DAN hydrochloride was prepared according to the literature[25], and a more detailed procedure was provided in the Supporting Information. Negative MALDI-MSI experiments were performed on an Autoflex Speed MALDI-TOF/TOF MS (Bruker Daltonics, Billerica, MA, USA) equipped with a smartbeam-II Nd: A YAG 355-nm laser. For more detailed parameters see Supporting Information.

2.5. Data processing and analysis

The procedure for processing and analysis of AFADESI-MSI data was referred to our previous work[24]. Briefly, ion image was constructed using custom-developed high-performance imaging software (MassImager 2.0, Beijing, China) with a bin width of $\Delta m/z = 0.005$. Average AFADESI-MS profiles from regions of interest (ROIs) were extracted by comparing with H&E stain images of the adjacent renal section, generating separate two-dimensional data matrixes (m/z, intensity) in.txt format. After background deduction, peak picking, and peak alignment performed using Markerview™ software 1.2.1 (AB SCIEX, Toronto, Ontario, Canada), total ion current (TIC) normalization was used to calculate the relative intensity of ions in each ROI. The processed datasets from different ROIs were compared by supervised multivariate orthogonal partial least squares discriminant analysis (OPLS-DA) to find differentiating metabolites associated with DN. More details were provided in Supporting Information.

MALDI-MSI data was processed by SCiLS Lab version 2016b (SCiLS, Bremen, Germany). The signal intensity of ROIs was compared using analysis of variance to get the metabolic differences between the control and DN groups, and $P < 0.05$ indicated statistical significance.

Provisional structural assignment of the discriminating metabolites was initially conducted by searching the public databases using exact molecular weights and interpreting of isotope patterns. Then, high-resolution LC–MS/MS analysis of kidney homogenates were conducted to get structural information based on the interpretation of the metabolites' fragmentation patterns and database searches. The detailed operation process for LC–MS/MS experiments was provided in the Supporting Information.

2.6. Western blot assay

Western blotting assay of phosphorylated adenosine monophosphate activated protein kinase (p-AMPK) were provided in the Supporting Information.

3. Results

3.1. Physiological, biochemical, and histopathological analyses

Body weight, food consumption, and water consumption for rats in the control, DN, L-AST, and H-AST groups are summarized in Supporting Information Fig. S1. Compared with the findings in the control group, DN group rats exhibited reduced body weight and food consumption and increased water consumption. There were no significant differences in these parameters after AST treatment for 12 weeks.

The blood and urinary biochemical indicators were shown in Supporting Information Fig. S2. The concentrations of blood glucose, HbA1c, blood urea nitrogen, uric acid, and triglyceride were significantly increased in the DN group (Fig. S2A−S2D and G), whereas those of serum albumin and total protein were significantly decreased (all $P < 0.05$) (Fig. S2L and S2M). Serum creatinine and cholesterol levels were marginally increased (both $P < 0.1$) in the DN group (Figs. S2E and S2F). The levels of urinary creatinine, Na^+, and Cl^- were significantly lower (all $P < 0.05$) in the DN group than in the control group (Fig. S2H, S2I and S2K). Blood urea nitrogen, uric acid, and serum creatinine, triglyceride, and cholesterol levels were slightly decreased after AST treatment, especially in the H-AST group.

Kidney weight, kidney/body weight ratio, and representative photomicrographs of H&E-stained kidney tissues are presented in Fig. 2. Kidney weight and the kidney/body weight ratio were significantly higher in the DN group than in the control group (Fig. 2A and B). Histological examination of H&E-stained kidney tissues revealed renal hypertrophy and glomerulus enlargement in rats in the DN group (Fig. 2C and D). The kidney/body weight ratio was significantly decreased and renal histological lesions were ameliorated in the H-AST group compared with the findings in the DN group.

These biological and pathological alterations suggested that renal injury occurred in untreated diabetic rats, and high-dose AST exerted protective effects on the kidneys of these animals.

3.2. AFADESI-MSI analysis of diabetic rat kidneys

The stability of the AFADESI-MSI system was evaluated by analysis of adjacent renal sections. As shown in Supporting Information Fig. S3, similar ion images were observed, suggesting the reproducibility of the AFADESI-MSI approach was suitable for *in situ* metabolomics study.

AFADESI-MS data of renal cortex, renal outer medulla, renal inter medulla, and whole renal section showed distinct separation on the OPLS-DA scatter plot (Supporting Information Fig. S4), suggesting different metabolic profiles of these morphology regions from the control, DN, and AST-treated groups. The OPLS-DA scatter plot (Supporting Information Fig. S5) also revealed that the renal cortex, outer medulla, and inter medulla of rats in the DN group could be clearly separated from those of rats in the control group, implying that distinguished metabolic alterations occurred in these regions in rats with STZ-induced diabetes. Forty-one and 19 that metabolites contributed most to the class separation were provisionally identified in negative and positive AFADESI-MSI analysis, respectively (Supporting Information Tables S1 and S2). These changed metabolites are related to metabolism of sugars, amino acids, organic acids, nucleotides and their derivatives, fatty acids, glycerides, phospholipids, sphingolipids, carnitine and its derivatives, vitamins, and peptides,

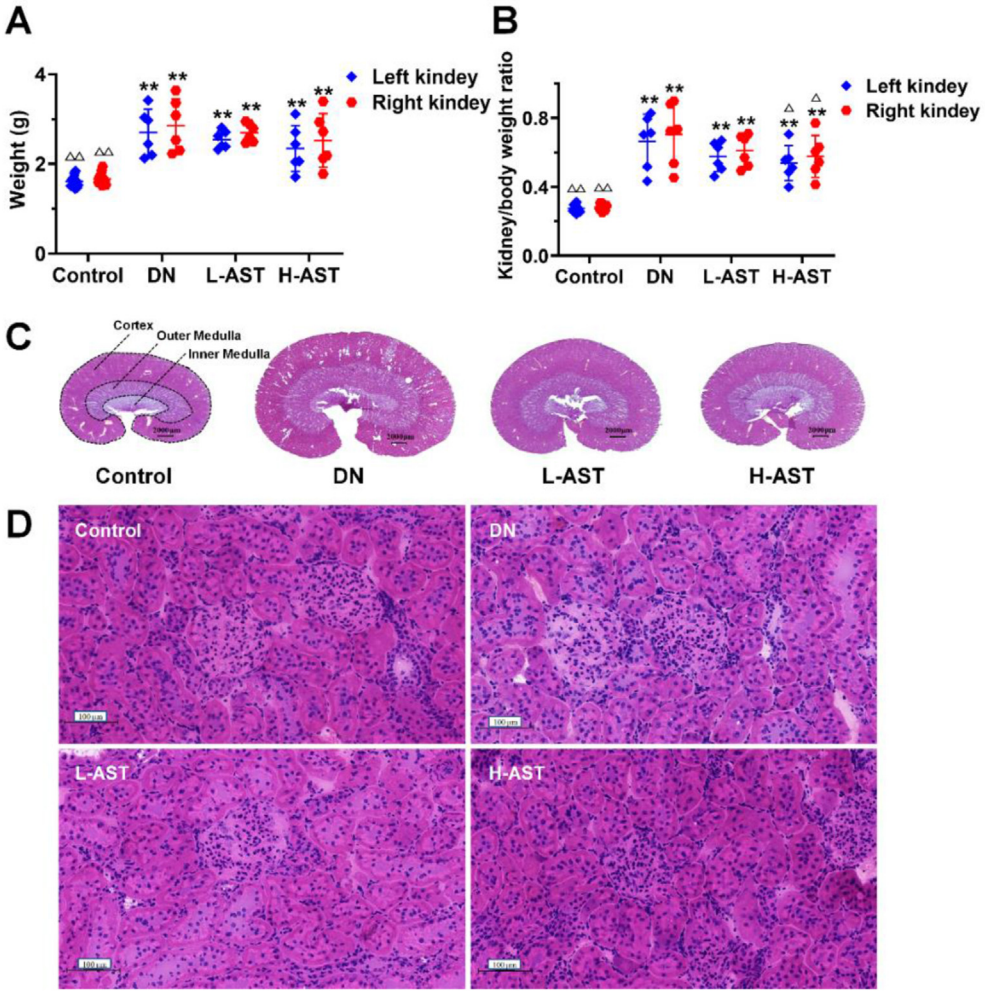

Figure 2 Kidney weight (A), and kidney/body weight ratio (B), and hematoxylin and eosin image of whole kidney sections (C) and renal cortex with a 20-fold magnification (D) in the control, DN, L-AST, and H-AST groups. Control: control group; DN: diabetic nephropathy group; L-AST: low-dose astragaloside IV (20 mg/kg) group; H-AST: high-dose astragaloside IV (100 mg/kg) group. $^{*}P \leq 0.05$, $^{**}P \leq 0.01$ compared with the control group; $^{\Delta}P \leq 0.05$, $^{\Delta\Delta}P \leq 0.01$ compared with the DN group. Data are presented as means ± standard deviation (SD), $n = 6$. Scale = 100 μm.

indicating extensive metabolic disorders can be detected by *in situ* AFADESI-MSI analysis in a tissue specific manner.

3.3. *MALDI-MSI analysis of diabetic rat kidneys*

MALDI-MS profiling of kidney sections from rats in the control and DN groups was further performed to more comprehensively investigate the metabolic changes in diabetic kidneys. Ten discriminating metabolites and one metal ion were tentatively identified (Supporting Information Table S3). Most of the metabolites (excluding adenosine triphosphate (ATP)), including adenosine monophosphate (AMP), Adenosine diphosphate (ADP), sorbitol, glucose, glyceraldehyde 3-phosphate, glutathione, citric acid, succinic acid, and ascorbic acid, matched the discriminating metabolites identified *via* AFADESI-MS analysis.

High-spatial-resolution MALDI-MSI was then performed to investigate the distribution of the discriminating metabolites identified using both AFADESI-MSI and MALDI-MSI profiling across the renal cortex, which was abundant in glomeruli and vulnerable to diabetic kidney damage. MALDI-MSI at a resolution of 20 μm clearly revealed a more precise distribution of the discriminating metabolites in the renal cortex. For example, phosphatidylserine (PS(36:2)) at *m/z* 786.5315 was distributed exclusively in the glomeruli, phosphatidylethanolamine (PE(38:6)) at *m/z* 762.5103 was distributed around the glomeruli, and AMP at *m/z* 346.0567 was distributed in other areas of the cortex (Fig. 3). The high-resolution MALDI-MS images of other metabolites were provided in Supporting Information Fig. S6.

4. Discussion

4.1. *Metabolic disturbances in the kidneys of diabetic rats*

4.1.1. *Disturbance of glucose metabolism pathways*

The spatial distribution and changes of metabolites involved in glucose metabolism are presented in Fig. 4. Glucose is the main energy substrate for the kidneys, which utilizes approximately 10% of all glucose available in the body[26,27]. The fate of glucose varies in different regions of the kidneys. Because of its low oxygen availability, low levels of oxidative enzymes, and high levels of glucose-phosphorylating enzymes, the renal medulla is considered an obligate utilizer of glucose for its energy requirement. Conversely, the renal cortex has little glucose-

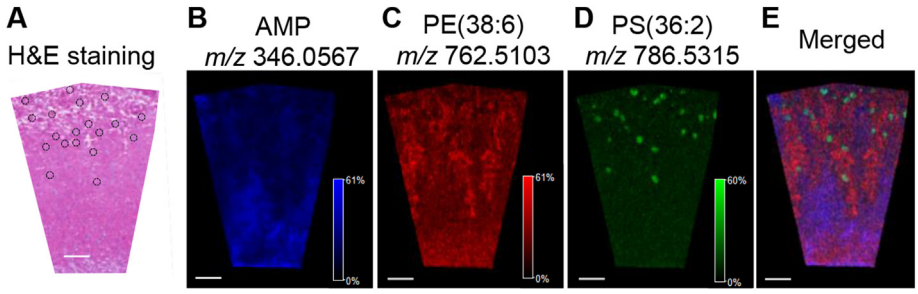

Figure 3 High-resolution matrix-assisted laser desorption ionization-mass spectrometry imaging (MALDI-MSI) of adenosine monophosphate (AMP) at *m/z* 346.0567, phosphatidylethanolamine (PE(38:6)) at *m/z* 762.5103, and phosphatidylserine (PS(36:2)) at *m/z* 786.5315 in the renal cortex. (A) Hematoxylin and eosin-stained image of the renal cortex. The dark circle indicates the glomerulus. (B−D) Ion images of AMP at *m/z* 346.0567, PE(38:6) at *m/z* 762.5103, and PS(36:2) at *m/z* 786.5315. (E) The merged image of B, C, and D. The MALDI-mass spectrometry images acquired at a spatial resolution of 20 μm. Scale bar: 500 μm.

phosphorylating capacity but a high level of oxidative enzymes, and thus, it can oxidize free fatty acids as its main source of energy[28]. In this study, the highest concentration of glucose was observed in the renal outer medulla in the control group, perhaps because of the extensive resorption and utilization of glucose in this region, in which sodium-glucose cotransporters (SGLTs) are predominantly distributed[29]. Glucose levels were significantly increased in the renal cortex of DN rats, which was consistent with the increase of system glucose content. However, glucose levels in the renal outer medulla were significantly lower in DN rats than in control rats. In addition, glucose 6-phosphate and glyceraldehyde 3-phosphate levels in the renal outer medulla were significantly higher in DN rats than in control rats. These results indicated that the overutilization of glucose and increased metabolic flux of glucose into the glycolytic pathway and pentose phosphate pathway (PPP) were occurring in the renal outer medulla[6,30].

Glucose also can be metabolized by sorbitol dehydrogenase to produce sorbitol, the levels of which were also significantly

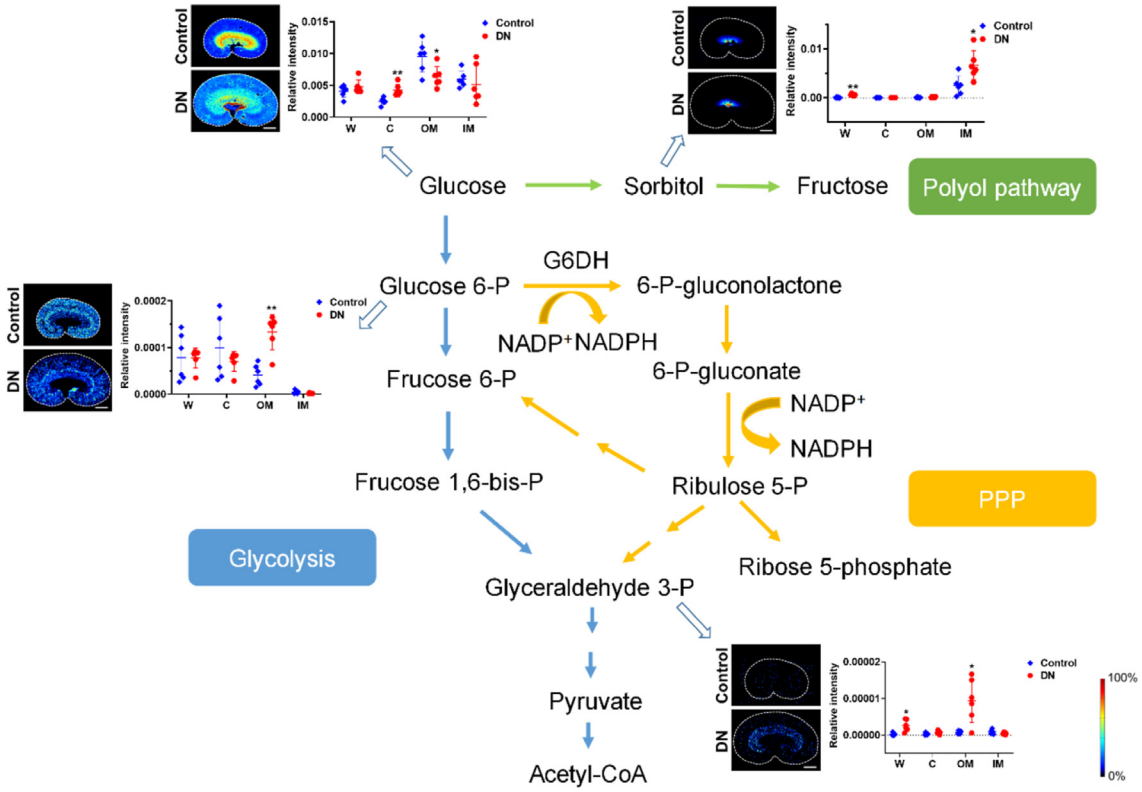

Figure 4 Air flow-assisted desorption electrospray ionizationmass spectrometry imaging of metabolites involved in glucose metabolism pathways in the kidneys in the control group and diabetic nephropathy groups. W: whole renal section; C: renal cortex; OM: renal outer medullar; IM: inner medullar; Control: control group; DN: diabetic nephropathy group; Glucose 6-P: glucose-6-phosphate; NADPH: nicotinamide adenine dinucleotide phosphate; G6DH: glucose 6-phosphate dehydrogenase; 6-P-gluconolactone: 6-phosphogluconolactone; 6-P-gluconate: 6-phosphogluconate; Ribulose 5-P: ribulose 5-phosphate; Glyceraldehyde 3-P: glyceraldehyde 3-phosphate; Acetyl-CoA: acetyl-coenzyme A; PPP: pentose phosphate pathway. Scale bar: 4 mm. $^{*}P \leq 0.05$, $^{**}P \leq 0.01$. Data are presented as means ± standard deviation (SD), $n = 6$.

elevated in the renal cortex and inner medulla in diabetic rats. The accumulation of sorbitol suggested increased metabolic flux of glucose into the polyol pathway in the kidneys, which is reportedly involved in the pathogenesis of DN[6].

4.1.2. Disorder of the tricarboxylic acid (TCA) cycle

The spatial distribution and changes of metabolites involved in the TCA cycle are presented in Fig. 5. Citric acid and malate are well-known intermediates in the TCA cycle. Their levels were significantly decreased in DN rats compared with those in control rats. Succinate is another important intermediate in the TCA cycle and a substrate of succinate dehydrogenase (SDH), which is part of the electron transport chain in the mitochondrial membrane and can catalyst succinate to form fumarate. Succinate levels in the renal outer medulla were higher in DN rats than in control rats. The levels of amino acids related to the TCA cycle, including glutamine, aspartate, threonine, and leucine/isoleucine, were also significantly decreased in the kidneys of DN rats. The disturbance of these TCA intermediates and TCA cycle-related metabolites indicated a reduction in SDH activity and mitochondrial dysfunction in the kidneys of DN rats, which have been identified as important contributors to the development in several diabetic complications[31,32].

4.1.3. Disruption of nucleotide metabolism

The spatial distribution and changes of metabolites involved in nucleotide metabolism are presented in Fig. 6. AMP, ADP, and guanosine monophosphate (GMP) were mainly distributed in the renal outer medulla in the control rats. However, the distribution patterns of these metabolites were changed significantly in the diabetic state. For AMP and GMP, there were remarkable decreases in their levels in the renal outer medulla but significantly increases in their levels in the renal cortex in the diabetic state. Concerning ADP and ATP, remarkable increases in their levels in both the renal cortex and outer medulla were observed in diabetic rats, indicating the accelerated turnover of ATP in these regions, which may be associated with hyperfunction of the kidneys, such as increases in the glomerular filtration rate and Na^+ and water resorption and altered Na^+/K^+ ATPase pump activity, in the diabetic state[33].

The AMP/ATP ratio was also calculated using the MALDI-MSI data (Fig. 6) because it is suspected to regulate the activity of AMP-activated protein kinase (AMPK), which is a major cellular energy sensor that plays an important role in the regulation of glucose and lipid metabolism[34]. The AMP/ATP ratio was significantly lower in the outer medulla but remarkably higher in cortex region when comparing DN and control, indicating different states of energy metabolism in these two regions. However, the decreased expression of phosphorylated AMPK (p-AMPKα) as determined using Western blotting revealed suppressed AMPK activity in both the renal cortex and medulla (Supporting Information Fig. S7). These results suggested that the activation of AMPK is complicated, and the AMP/ATP ratio alone may be unable to activate this signaling pathway[35,36]. AMPK dysfunction may result in reduced mitochondrial function in diabetic kidneys and play an important role in the development of DN[37].

Inosine, hypoxanthine, xanthine, uric acid, and uridine, which are catabolic products of AMP, GMP, and uridine monophosphate (UMP), were mainly distributed in the renal cortex in the control group. The levels of these metabolites tended to be decreased in

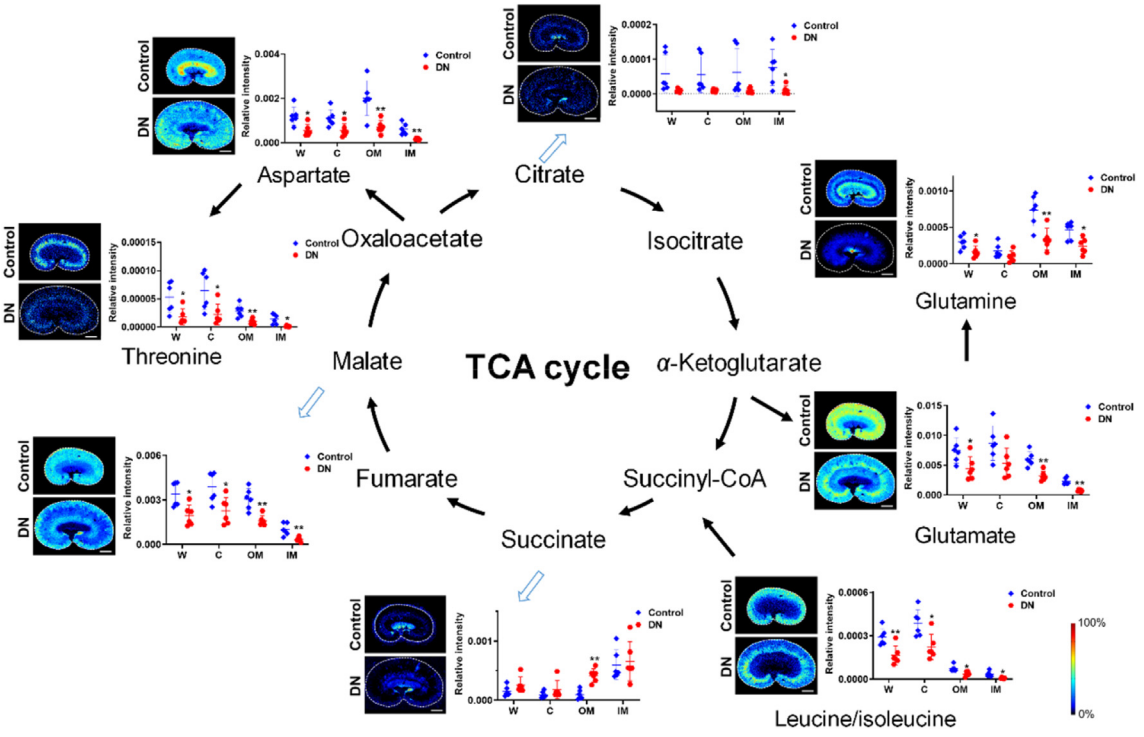

Figure 5 Air flow-assisted desorption electrospray ionization-mass spectrometry imaging of metabolites involved in tricarboxylic acid (TCA) cycle in the kidneys of control and diabetic nephropathy rats. W: whole renal section; C: renal cortex; OM: renal outer medullar; IM: inner medullar; Control: control group; DN: diabetic nephropathy group; Succinyl-CoA: succinyl coenzyme A. Scale bar: 4 mm. $^*P \leq 0.05$, $^{**}P \leq 0.01$. Data are presented as means ± standard deviation (SD), $n = 6$.

the kidneys of DN rats, suggesting reduced AMP, GMP, and UMP catabolism.

4.1.4. *Dysregulation of lipid metabolism*

In this study, we observed variable changes in levels and spatial distributions of a variety of metabolites related to lipids homeostasis, including fatty acids, lysophosphatidylcholine (LysoPC), lysophosphatidylglycerol (LysoPG), phosphatidic acid (PA), diacylglycerol (DAG), phosphatidylcholine (PC), PE, PS, and sphingomyelin (SM) in the kidney of DN rats (Fig. 7).

The concentration of oleic acid was significantly elevated in the renal cortex in DN group. Conversely, the levels of polyunsaturated fatty acids (PUFAs), including linolenic acid, linoleic acid, arachidonic acid, eicosapentaenoic acid, docosahexaenoic acid, and docosapentaenoic acid (DPA) (Fig. 7B2−B7), which were mainly distributed in the renal cortex in the control group, tended to be decreased in different regions of the kidneys in the diabetic state, excluding DPA in the renal outer medulla. The accumulation of oleic acid in renal cortex can reportedly activate peroxisome proliferator-activated receptors (PPARs) and induce renal injury[38]. PUFAs are the major components of the plasma membrane and the precursors of prostaglandins and leukotrienes. It has been reported that PUFAs exert anti-inflammatory effects in several diseases including DN[39]. The elevated oleic acid levels and decreased PUFAs levels suggested that increased renal inflammation may be happening in the kidney of DN rats[40].

We observed a heavy deposition of DAG(18:1/18:1), DAG(18:1/18:2), PC(32:0), PC(34:1), PC(36:2), PC(36:1), PC(38:4), PC(38:5), and LysoPC(16:0) across the renal section, especially in the outer medullar, in the DN group (Fig. 7B8−B15

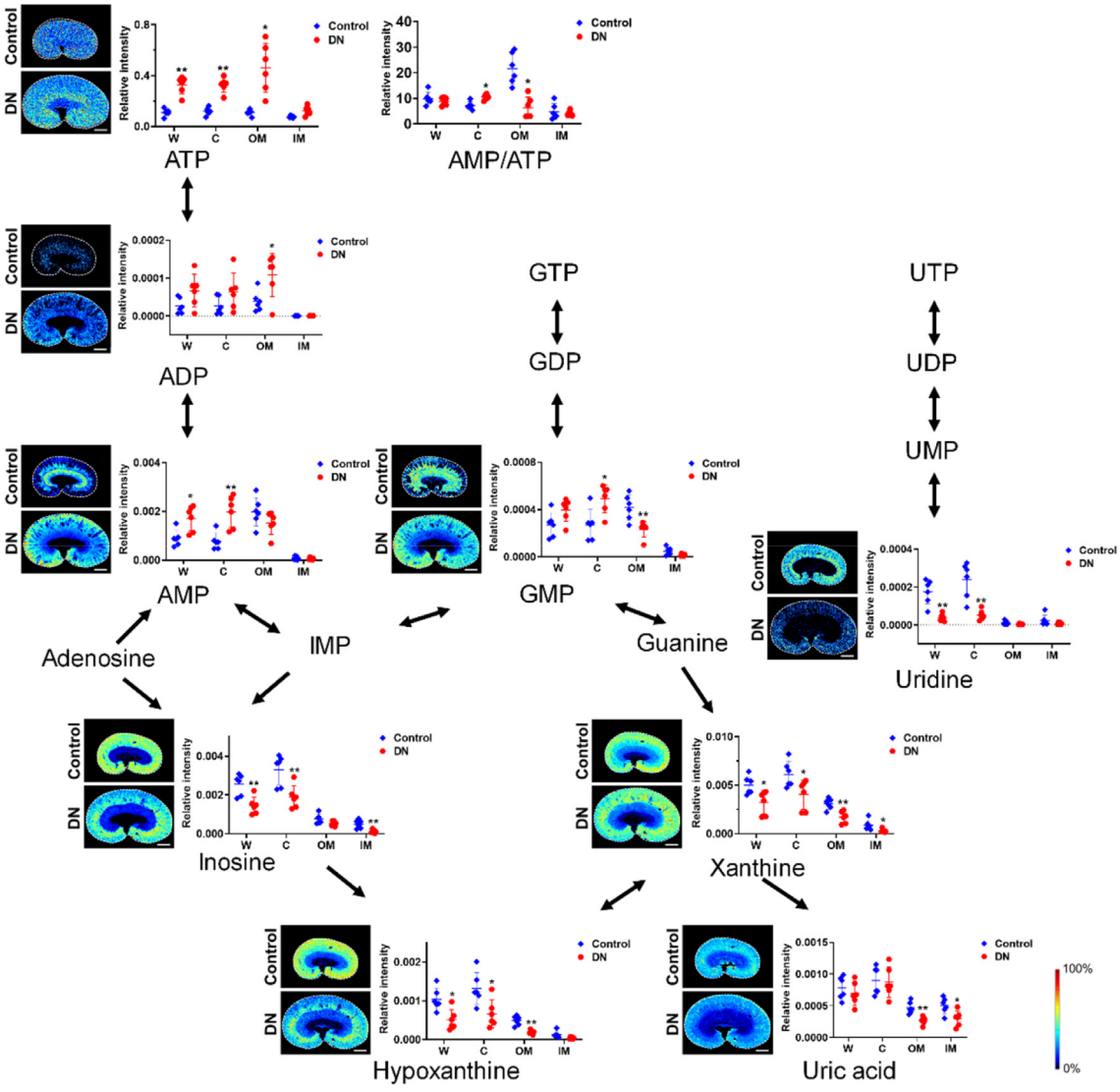

Figure 6 Air flow-assisted desorption electrospray ionization- and matrix-assisted laser desorption ionization-mass spectrometry imaging of metabolites involved in nucleotide metabolism in the kidneys of rats in the control and diabetic nephropathy groups. W: whole renal section; C: renal cortex; OM: renal outer medullar; IM: inner medullar; Control: control group; DN: diabetic nephropathy group; AMP: adenosine monophosphate, ADP: adenosine diphosphate, ATP: adenosine triphosphate; GTP: guanosine triphosphate; GDP: guanosine diphosphate; UTP: uridine triphosphate; UDP: uridine diphosphate; UMP: uridine monophosphate; IMP: inosine monophosphate. Scale bar: 4 mm. $^{*}P \leq 0.05$, $^{**}P \leq 0.01$. Data are presented as means ± standard deviation (SD), $n = 6$.

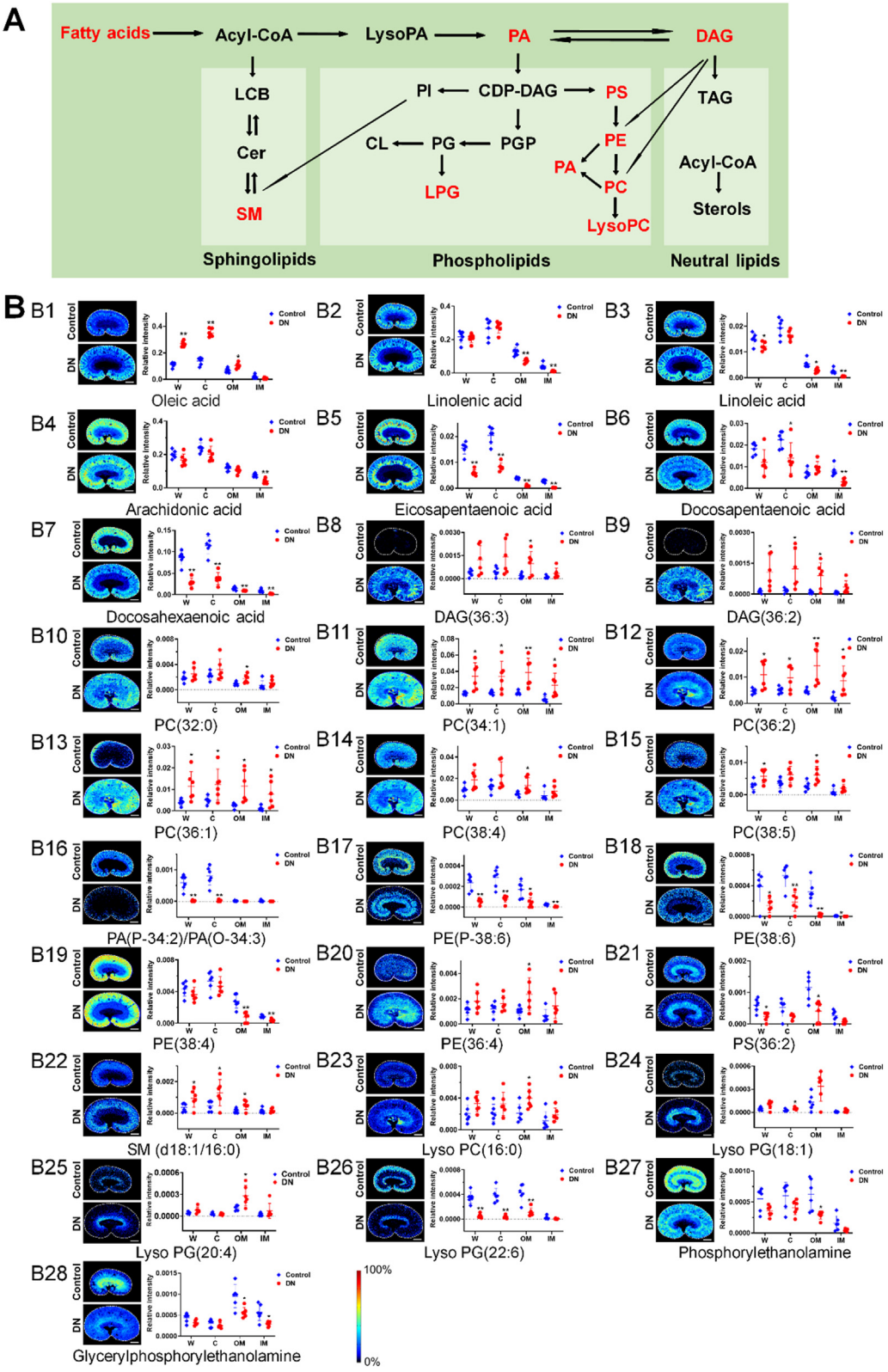

Figure 7 (A) Simplified overview of lipid metabolism. (B) Air flow-assisted desorption electrospray ionization-mass spectrometry imaging of metabolites involved in lipid metabolism in the kidneys in rats in the control and diabetic nephropathy groups. W: whole renal section; C: renal cortex; OM: renal outer medullar; IM: inner medullar; Control: control group; DN: diabetic nephropathy group; CDP-DAG: cytidine diphosphate-diacylglycerol; Cer: ceramides; DAG: diacylglycerol: LCB: long-chain sphingoid bases; LysoPC: lysophosphatidylcholine; LysoPG: lysophosphatidylglycerol; PA: phosphatidic acid; PC: phosphatidylcholine; PE: phosphatidylethanolamine; PG: phosphatidylglycerol; PGP: phosphatidylglycerophosphate; PI: phosphatidylinositol; PS: phosphatidylserine; SM: sphingomyelin; TAG: triacylglycerol. The red fonts represent changed metabolites in this study. Scale bar: 4 mm. $*P \leq 0.05$, $**P \leq 0.01$. Data are presented as means ± standard deviation (SD), $n = 6$.

and B23). The effect of renal lipid deposition in the kidney is well recognized in both animal models of DN and human diabetic nephropathy, where lipids accumulate in the kidney and are associated with glomerulosclerosis and tubulointerstitial damage[41]. Lipid deposition and lipotoxicity seems to contribute to insulin resistance, dysfunction and apoptosis of podocyte. LysoPC(16:0) can reportedly promote the expression of chemokines and adhesion molecules in glomerular cells, resulting recruitment of macrophage and inflammation[42]. The accumulation of lipid in kidney may be related to the dysfunction of lipid metabolism genes[41].

LysoPG(18:1) and LysoPG(20:4) levels were significantly increased in the renal outer medulla and LysoPG(22:6) levels were significantly decreased in the renal cortex and outer medulla in the DN group (Fig. 7B24−B26). In addition, the levels of PA(P-34:2)/PA(O-34:3), which were exclusively distributed in the renal cortex, were also significantly decreased in the diabetic group (Fig. 7B16). LysoPG and PA are important intermediates for the biosynthesis and remodeling of cardiolipin (CL), a phospholipid that is uniquely distributed in the inner mitochondrial membrane, in which it participates in oxidative phosphorylation and ATP synthesis[43]. The biological functions of CL are believed to depend on its acyl chain composition, which can be regulated by CL remodeling to incorporate appropriate acyl groups[43]. Alterations of LysoPG and PA levels may induce the pathological remodeling of CL, which has been considered responsible for the etiology of mitochondrial dysfunction-associated diabetes[43,44].

The levels of PE(P-38:6), PE(38:6), PE(38:4), phosphorylethanolamine, and glycerylphosphorylethanolamine, which are precursors of PE, were significantly decreased in the kidneys of DN rats (Fig. 7B17−B19, B27 and B28). However, the levels of PE(36:4) were significantly increased in the renal outer medullar of DN rats (Fig. 7B20). PE is the second most abundant mitochondrial phospholipid, and it can reportedly modulate ATP production and glucose metabolism[45]. Altered renal PE levels may result in decreased electron transport chain complex activities, respiratory capacity, and mitochondrial ATP production.

PS(36:2) levels were significantly decreased in the kidneys of DN rats (Fig. 7B21). High-resolution MALDI-MSI of PS(36:2) revealed its exclusive distribution in the glomeruli in the renal cortex (Fig. 3). PS is a quantitatively minor membrane phospholipid, and it can be metabolized to PE by PS decarboxylase in mitochondria[45]. PS has a normally asymmetric distribution across the membrane bilayer, and it regulates a variety of signaling pathways, such as the blood clotting cascade and apoptosis[46]. The specific distribution of PS(36:2) in the glomeruli suggests that it may play an important biological role in diabetic glomerulosclerosis, which may be a novel therapeutic targets for diabetic nephropathy.

SM(d18:1/16:0) showed a predominant distribution in renal cortex in control group, but were significantly increased in the renal cortex and outer medullar in DN group (Fig. 7B22). SM is one of the major phospholipids of membrane microdomains such as s lipid raft, caveolae, and clathrin-coated pits, which play an important role in lipid uptake and glucose homeostasis[47,48]. Previous studies suggest that the accumulation of sphingomyelin and may play a key role in the etiology of kidney disease in type 1 diabetes[30,49]. The accumulation of SM(d18:1/16:0) in the renal cortex and outer medullar may inhibit AMPK activity and contribute to lipid deposition[48].

4.1.5. *Disturbance of carnitine homeostasis*

Carnitine play an indispensable role in the regulation of mitochondrial oxidation of fatty acids and the acyl-CoA/CoA ratio, which in turn modulates multiple mitochondrial enzymes involved in TCA cycle[50]. Dysregulation of carnitine homeostasis is generally assumed to be associated in the development of DN. However, the results are reportedly controversial[50]. In this study, we observed a significant changed renal carnitine profiles in the DN rat. As shown in Fig. 8, L-carnitine and short-chain acylcarnitines, including acetylcarnitine and acylcarnitine C4:0, were detected with high intensity in the cortex and outer medullar in the control group, but significantly decreased in renal cortex in DN group (Fig. 8A and C). Long-chain acylcarnitines, including acylcarnitine C14:0, acylcarnitine C16:1, acylcarnitine C16:0, acylcarnitine C18:1, and acylcarnitine C18:0, were mainly distributed in the renal outer medulla in the control group, but showed a remarkable accumulation across the kidneys of DN (Fig. 8D−H). The altered renal carnitine profiles may be related to the dysfunction of mitochondrial acid oxidation and altered tricarboxylic acid cycle activity in DN[51].

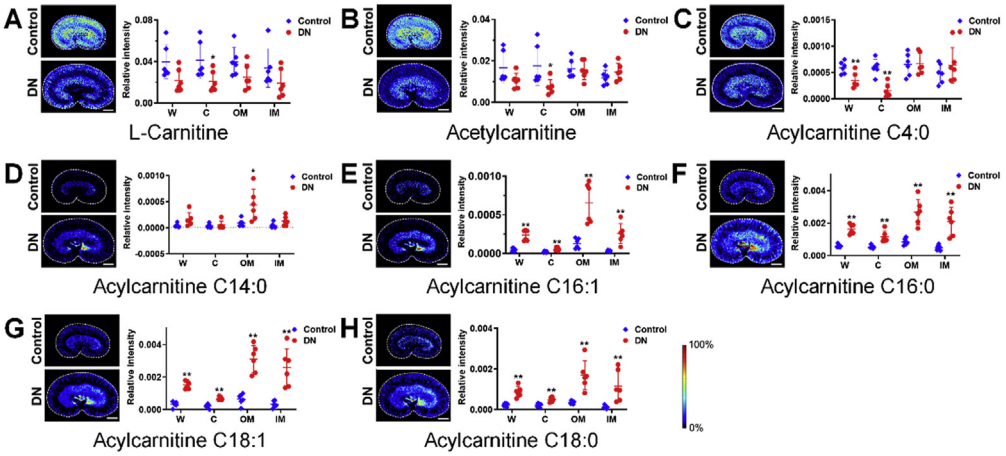

Figure 8 Air flow-assisted desorption electrospray ionization-mass spectrometry imaging of L-canitine and its derivatives in the kidneys of rats in the control and diabetic nephropathy groups. W: whole renal section; C: renal cortex; OM: renal outer medullar; IM: inner medullar; Control: control group; DN: diabetic nephropathy group. Scale bar: 4 mm. $^{*}P \leq 0.05$, $^{**}P \leq 0.01$. Data are presented as means ± standard deviation (SD), $n = 6$.

4.1.6. *Disruption of redox and sodium homeostasis*

Extensive investigations have been performed on the role of reactive oxygen species (ROS) in the development of DN, but these results were inconsistent[37,52–57]. Currently, a common belief is that hyperglycemia can lead to the overproduction of ROS and oxidative stress. In particular, it was generally believed that mitochondrial superoxide is a major contributor to diabetic complications[56,57]. However, anti-oxidant-based therapy in patients with DN has proven to be largely ineffective[52,57]. Moreover, recent studies reported that the overall renal O_2^- production was reduced along with a reduction in mitochondrial function in rats with STZ-induced diabetes[37], and restoring mitochondrial superoxide levels could protect *db*/*db* mice against progression of diabetic kidney disease[58]. In the study, ascorbic acid, taurine, and glutathione exhibited region-specific and complementary distribution patterns among the renal sections in the control rats (Supporting Information Fig. S8). Ascorbic acid levels were highest in the inner medulla and lowest in the renal juxtamedullary cortex (Fig. S8A). Taurine levels were highest in the renal juxtamedullary cortex and lowest in the renal inner medulla (Fig. S8B). Glutathione (GSH) levels were highest in the renal outer medulla and lowest in the juxtamedullary cortex (Fig. S8C). These findings indicated that these compounds may exert their anti-oxidant effects in a region-specific manner. The concentrations of ascorbic acid and taurine were significantly decreased in the kidney of diabetic rats, indicating increased oxidative stress in diabetic kidneys[55,56]. However, the concentration of GSH was marginally elevated in the renal outer medulla in the diabetic group ($P < 0.1$). Renal GSH levels are maintained through the activity of glutathione reductase, which catalyzes the conversion of oxidized glutathione to GSH in an NADPH-dependent manner[6]. The increased GSH content may be associated with increased PPP activity in the renal outer medulla, which can result in the overproduction of NADPH[6], or mitochondrial dysfunction, which can result in reduced superoxide production[37]. These contradicting results indicate that oxidation−reduction reactions in diabetic kidneys are complicated, and redox homeostasis in the kidneys is significantly changed in the diabetic state.

The spatial distribution and changes in Na^+ levels are illustrated in Fig. S8D. Na^+ was mainly distributed in the renal medulla in the control group, and its levels were significantly elevated in the diabetic state. Conversely, a decreased urinary Na^+ level was observed in the diabetic state. The accumulation of Na^+ in the renal medulla indicted changes in the osmolality gradient, which may be one of the major causes of nephrohypertrophy[59,60].

The metabolic alteration and their potential association with DN are summarized in Supporting Information Fig. S9. These findings provide visual and detailed evidences supporting that AMPK and mitochondrial dysfunction may act as an important role in the pathogenesis of DN. These results may be explained by the fact that chronic hyperglycemia exposure may suppress the expression of AMPK, which would induce increased glycolysis and mitochondrial dysfunction, thereby causing alteration of disorder of TCA cycle, dysregulation of lipid metabolism, disturbance of carnitine homeostasis, reduced mitochondrial superoxide production, and disruption of redox homeostasis. In addition, increases of PPP, polyol pathway and sodium retention also contributed to the pathogenesis of DN. To the best of our knowledge, this is the first study to investigate and visualize the *in situ* metabolic reprograming in diabetic kidney covering a broad range of metabolites including sugars, amino acids, nucleotides and their derivatives, fatty acids, phospholipids, sphingolipids, glycerides, carnitine and its derivatives, vitamins, peptides, and metal ions.

4.2. *Metabolic impact of AST treatment on DN*

AST is the major component of the traditional Chinese medical herb *Astragalus membranaceus* (Fisch.). It exhibits multiple pharmacological effects including anti-inflammatory, anti-hypertensive cardioprotective, anti-oxidant, and anti-apoptotic activities[61]. Recent studies revealed that AST had a renoprotective effect in *db*/*db* mice, but the underlying mechanism remains incompletely elucidated[62]. As shown in Supporting Information Fig. S10, the disturbances of the levels of multiple metabolites were ameliorated by repeated oral administration of high-dose AST (100 mg/kg) for 12 weeks. AMP levels were significantly decreased in the renal cortex of rats in the H-AST group compared with those in control rats (Fig. S10A). ADP and GMP levels also tended to be lower in the renal cortex of AST-treated diabetic rats than in untreated diabetic rats (Fig. S8B and S8C). In addition, the disturbances of the levels of TCA cycle intermediates and related metabolites were slightly reversed, and glutathione levels was marginally decreased in diabetic rats after treatment with high-dose AST for 12 weeks (Fig. S10L). One possible explanation for these results is that high-dose AST may be able to activate AMPK, which was confirmed by the Western blotting result for p-AMPKα (Fig. S7), and thus improve the function of renal mitochondria in diabetic rats[63], promoting the metabolic shift from glycolysis and PPP to mitochondrial oxidative phosphorylation. This would promote TCA cycle turnover and thereby result in increased mitochondrial ATP synthesis, which may improve energy metabolism in kidneys of DN rats. The increased mitochondrial activity also would elevate the production of mitochondrial superoxide, resulting in reduced GSH levels.

The disturbances in the renal levels of arachidonic acid, DAG(36:2), DAG(36:3), PC(32:0), PC(34:1), PC(36:2), PC(36:1), PC(38:4), PC(38:5), PA(P-34:2)/PA(O-34:3), PE(36:4), PS(36:2), SM(d18:1/16:0), LysoPG(22:6), and LysoPC(16:0), and serum levels of cholesterol and triglyceride in rats in the DN group were also slightly reversed after treatment with high-dose AST for 12 weeks, indicating a potential role of AST in regulating lipid metabolism in DN[64] (Fig. S10N and O-AA and Fig. S2F and S2G).

5. Conclusions

In summary, a spatial-resolved metabolomics approach combing the strengths of AFADESI- and MALDI-MSI was proposed to investigate the region-specific metabolic alterations in diabetic kidney as well as the therapeutic effect of AST on DN. AFADESI-MSI identified a wide range of metabolites associated with DN and visualized their unique spatial distribution patterns in the rat kidney, while the addition of MALDI-MSI improved the spatial resolution of metabolites detected by AFADESI. The results suggested that increased glycolytic and PPP activity, mitochondrial dysfunction, AMPK inhibition, disorder of lipid metabolism, and disruption of carnitine, redox and osmotic homeostasis occurred in region-specific manner in the kidneys of DN rats. These region-specific metabolic disturbances were ameliorated by repeated oral administration of astragaloside IV (100 mg/kg) for 12 weeks. This study provided more comprehensive and detailed information about the tissue-specific metabolic reprogramming and molecular pathological signature in the kidney of diabetic rats.

The newly discovered glomerulus-specific discriminating metabolite PS(36:2) may be used to locate glomerulus and find glomerulus-specific biomarker for DN. These findings highlighted the powerful role of AFADESI and MALDI integrated MSI based metabolomics approach for application in metabolic kidney diseases.

Acknowledgments

This research was supported by the National Natural Science Foundation of China (No. 81803483, No. 21927808) and National Key Research and Development Program of China (No. 2017YFC1704006).

Author contributions

Zhonghua Wang, conceptualization, methodology, formal analysis, investigation, data curation, writing–original draft; Wenqing Fu, investigation, data curation, visualization, formal analysis, writing–original draft; Meiling Huo, investigation, data curation, formal analysis; Bingshu He, software, formal analysis; Yaqi Liu, formal analysis; Lu Tian, investigation; Wanfang Li, investigation; Zhi Zhou, validation; Baili Wang, resources; Jianzhen Xia, resources; Yanhua Chen, validation; Jinfeng Wei, supervision, project administration; Zeper Abliz, supervision, project administration, funding acquisition, writing–review & editing.

Conflicts of interest

The authors have no conflicts of interest to declare.

Appendix A. Supporting information

Supporting information data to this article can be found online at https://doi.org/10.1016/j.apsb.2021.05.013.

References

1. Zimmet PZ, Magliano DJ, Herman WH, Shaw JE. Diabetes: a 21st century challenge. *Lancet Diabetes Endocrinol* 2014;**2**:56–64.
2. Saeedi P, Petersohn I, Salpea P, Malanda B, Karuranga S, Unwin N, et al. Global and regional diabetes prevalence estimates for 2019 and projections for 2030 and 2045: results from the International Diabetes Federation Diabetes Atlas. 9th ed. *Diabetes Res Clin Pract* 2019;**157**:107843.
3. Thomas MC, Cooper ME, Zimmet P. Changing epidemiology of type 2 diabetes mellitus and associated chronic kidney disease. *Nat Rev Nephrol* 2016;**12**:73–81.
4. Gross JL, de Azevedo MJ, Silveiro SP, Canani LH, Caramori ML, Zelmanovitz T. Diabetic nephropathy: diagnosis, prevention, and treatment. *Diabetes Care* 2005;**28**:164–76.
5. Gheith O, Farouk N, Nampoory N, Halim MA, Al-Otaibi T. Diabetic kidney disease: world wide difference of prevalence and risk factors. *J Nephropharmacol* 2016;**5**:49–56.
6. Brownlee M. Biochemistry and molecular cell biology of diabetic complications. *Nature* 2001;**414**:813–20.
7. Dronavalli S, Duka I, Bakris GL. The pathogenesis of diabetic nephropathy. *Nat Clin Pract Endocrinol* 2008;**4**:444–52.
8. Sifuentes-Franco S, Padilla-Tejeda DE, Carrillo-Ibarra S, Miranda-Díaz AG. Oxidative stress, apoptosis, and mitochondrial function in diabetic nephropathy. *Internet J Endocrinol* 2018;**2018**:1875870.
9. Yiu WH, Wong DW, Wu HJ, Li RX, Yam I, Chan LY, et al. Kallistatin protects against diabetic nephropathy in *db/db* mice by suppressing AGE-RAGE-induced oxidative stress. *Kidney Int* 2016;**89**:386–98.
10. Umanath K, Lewis JB. Update on diabetic nephropathy: core curriculum. *Am J Kidney Dis* 2018;**71**:884–95.
11. Zhang J, Yan L, Chen W, Lin L, Song X, Yan X, et al. Metabonomics research of diabetic nephropathy and type 2 diabetes mellitus based on UPLC-oaTOF-MS system. *Anal Chim Acta* 2009;**650**:16–22.
12. Hirayama A, Nakashima E, Sugimoto M, Akiyama S, Sato W, Maruyama S, et al. Metabolic profiling reveals new serum biomarkers for differentiating diabetic nephropathy. *Anal Bioanal Chem* 2012;**404**:3101–9.
13. Zhao L, Gao H, Lian F, Liu X, Zhao Y, Lin D. ^{1}H-NMR-based metabonomic analysis of metabolic profiling in diabetic nephropathy rats induced by streptozotocin. *Am J Physiol Ren Physiol* 2011;**300**:F947–56.
14. Darshi M, Van Espen B, Sharma K. Metabolomics in diabetic kidney disease: unraveling the biochemistry of a silent killer. *Am J Nephrol* 2016;**44**:92–103.
15. Spengler B. Mass spectrometry imaging of biomolecular information. *Anal Chem* 2015;**87**:64–82.
16. Buchberger AR, DeLaney K, Johnson J, Li L. Mass spectrometry imaging: a review of emerging advancements and future insights. *Anal Chem* 2018;**90**:240–65.
17. Wu C, Dill AL, Eberlin LS, Cooks RG, Ifa DR. Mass spectrometry imaging under ambient conditions. *Mass Spectrom Rev* 2013;**32**:218–43.
18. Gessel MM, Norris JL, Caprioli RM. MALDI imaging mass spectrometry: spatial molecular analysis to enable a new age of discovery. *J proteomics* 2014;**107**:71–82.
19. Calvano CD, Monopoli A, Cataldi T, Palmisano F. MALDI matrices for low molecular weight compounds: an endless story?. *Anal Bioanal Chem* 2018;**410**:4015–38.
20. Morikawa-Ichinose T, Fujimura Y, Murayama F, Yamazaki Y, Yamamoto T, Wariishi H, et al. Improvement of sensitivity and reproducibility for imaging of endogenous metabolites by matrix-assisted laser desorption/ionization-mass spectrometry. *J Am Soc Mass Spectrom* 2019;**30**:1512–20.
21. He J, Sun C, Li T, Luo Z, Huang L, Song X, et al. A sensitive and wide coverage ambient mass spectrometry imaging method for functional metabolites based molecular histology. *Adv Sci* 2018;**5**:1800250.
22. Bergman HM, Lindfors L, Palm F, Kihlberg J, Lanekoff I. Metabolite aberrations in early diabetes detected in rat kidney using mass spectrometry imaging. *Anal Bioanal Chem* 2019;**411**:2809–16.
23. Miyamoto S, Hsu CC, Hamm G, Darshi M, Diamond-Stanic M, Declèves AE, et al. Mass spectrometry imaging reveals elevated glomerular ATP/AMP in diabetes/obesity and identifies sphingomyelin as a possible mediator. *EBioMedicine* 2016;**7**:121–34.
24. Wang Z, He B, Liu Y, Huo M, Fu W, Yang C, et al. *In situ* metabolomics in nephrotoxicity of aristolochic acids based on air flow-assisted desorption electrospray ionization mass spectrometry imaging. *Acta Pharm Sin B* 2020;**10**:1083–93.
25. Liu H, Chen R, Wang J, Chen S, Xiong C, Wang J, et al. 1,5-Diaminonaphthalene hydrochloride assisted laser desorption/ionization mass spectrometry imaging of small molecules in tissues following focal cerebral ischemia. *Anal Chem* 2014;**86**:10114–21.
26. Gerich JE. Physiology of glucose homeostasis. *Diabetes Obes Metabol* 2000;**2**:345–50.
27. Meyer C, Dostou JM, Welle SL, Gerich JE. Role of human liver, kidney, and skeletal muscle in postprandial glucose homeostasis. *Am J Physiol Endocrinol Metab* 2002;**282**:E419–27.
28. Gerich JE. Role of the kidney in normal glucose homeostasis and in the hyperglycaemia of diabetes mellitus: therapeutic implications. *Diabet Med* 2010;**27**:136–42.
29. Balen D, Ljubojevic M, Breljak D, Brzica H, Zlender V, Koepsell H, et al. Revised immunolocalization of the Na^{+}-D-glucose cotransporter SGLT1 in rat organs with an improved antibody. *Am J Physiol Cell Physiol* 2008;**295**:C475–89.

30. Zhang G, Darshi M, Sharma K. The warburg effect in diabetic kidney disease. *Semin Nephrol* 2018;**38**:111−20.
31. Forbes JM, Thorburn DR. Mitochondrial dysfunction in diabetic kidney disease. *Nat Rev Nephrol* 2018;**14**:291−312.
32. Hallan S, Sharma K. The role of mitochondria in diabetic kidney disease. *Curr Diab Rep* 2016;**16**:61.
33. Katyare SS, Satav JG. Effect of streptozotocin-induced diabetes on oxidative energy metabolism in rat kidney mitochondria. A comparative study of early and late effects. *Diabetes Obes Metabol* 2005;**7**:555−62.
34. Lin SC, Hardie DG. AMPK: sensing glucose as well as cellular energy status. *Cell Metabol* 2018;**27**:299−313.
35. Emerling BM, Weinberg F, Snyder C, Burgess Z, Mutlu GM, Viollet B, et al. Hypoxic activation of AMPK is dependent on mitochondrial ROS but independent of an increase in AMP/ATP ratio. *Free Radic Biol Med* 2009;**46**:1386−91.
36. Fryer LG, Parbu-Patel A, Carling D. The anti-diabetic drugs rosiglitazone and metformin stimulate AMP-activated protein kinase through distinct signaling pathways. *J Biol Chem* 2002;**277**:25226−32.
37. Dugan LL, You YH, Ali SS, Diamond-Stanic M, Miyamoto S, DeCleves AE, et al. AMPK dysregulation promotes diabetes-related reduction of superoxide and mitochondrial function. *J Clin Invest* 2013;**123**:4888−99.
38. Rodríguez-Iturbe B, García GG. The role of tubulointerstitial inflammation in the progression of chronic renal failure. *Nephron Clin Pract* 2010;**116**:c81−8.
39. Shapiro H, Theilla M, Attal-Singer J, Singer P. Effects of polyunsaturated fatty acid consumption in diabetic nephropathy. *Nat Rev Nephrol* 2011;**7**:110−21.
40. Duran-Salgado MB, Rubio-Guerra AF. Diabetic nephropathy and inflammation. *World J Diabetes* 2014;**5**:393−8.
41. Herman-Edelstein M, Scherzer P, Tobar A, Levi M, Gafter U. Altered renal lipid metabolism and renal lipid accumulation in human diabetic nephropathy. *J Lipid Res* 2014;**55**:561−72.
42. Miyazaki K, Isbel NM, Lan HY, Hattori M, Ito K, Bacher M, et al. Up-regulation of macrophage colony-stimulating factor (M-CSF) and migration inhibitory factor (MIF) expression and monocyte recruitment during lipid-induced glomerular injury in the exogenous hypercholesterolaemic (ExHC) rat. *Clin Exp Immunol* 1997;**108**:318−23.
43. Shi Y. Emerging roles of cardiolipin remodeling in mitochondrial dysfunction associated with diabetes, obesity, and cardiovascular diseases. *J Biomed Res* 2010;**24**:6−15.
44. Ducasa GM, Mitrofanova A, Fornoni A. Crosstalk between lipids and mitochondria in diabetic kidney disease. *Curr Diab Rep* 2019;**19**:144.
45. van der Veen JN, Lingrell S, Da SR, Jacobs RL, Vance DE. The concentration of phosphatidylethanolamine in mitochondria can modulate ATP production and glucose metabolism in mice. *Diabetes* 2014;**63**:2620−30.
46. Vance JE, Steenbergen R. Metabolism and functions of phosphatidylserine. *Prog Lipid Res* 2005;**44**:207−34.
47. Taniguchi M, Okazaki T. The role of sphingomyelin and sphingomyelin synthases in cell death, proliferation and migration-from cell and animal models to human disorders. *Biochim Biophys Acta* 2014;**1841**:692−703.
48. Mitsutake S, Zama K, Yokota H, Yoshida T, Tanaka M, Mitsui M, et al. Dynamic modification of sphingomyelin in lipid microdomains controls development of obesity, fatty liver, and type 2 diabetes. *J Biol Chem* 2011;**286**:28544−55.
49. Pongrac BD, Harjutsalo V, Sandholm N, Forsblom C, Groop PH. Sphingomyelin and progression of renal and coronary heart disease in individuals with type 1 diabetes. *Diabetologia* 2020;**63**:1847−56.
50. Bene J, Hadzsiev K, Melegh B. Role of carnitine and its derivatives in the development and management of type 2 diabetes. *Nutr Diabetes* 2018;**8**:8.
51. Adams SH, Hoppel CL, Lok KH, Zhao L, Wong SW, Minkler PE, et al. Plasma acylcarnitine profiles suggest incomplete long-chain fatty acid beta-oxidation and altered tricarboxylic acid cycle activity in type 2 diabetic African-American women. *J Nutr* 2009;**139**:1073−81.
52. Vasavada N, Agarwal R. Role of oxidative stress in diabetic nephropathy. *Adv Chronic Kidney Dis* 2005;**12**:146−54.
53. Geiszt M, Kopp JB, Várnai P, Leto TL. Identification of renox, an NAD(P)H oxidase in kidney. *Proc Natl Acad Sci U S A* 2000;**97**:8010−4.
54. He L, He T, Farrar S, Ji L, Liu T, Ma X. Antioxidants maintain cellular redox homeostasis by elimination of reactive oxygen species. *Cell Physiol Biochem* 2017;**44**:532−53.
55. Fiorentino TV, Prioletta A, Zuo P, Folli F. Hyperglycemia-induced oxidative stress and its role in diabetes mellitus related cardiovascular diseases. *Curr Pharm Des* 2013;**19**:5695−703.
56. Nishikawa T, Brownlee M, Araki E. Mitochondrial reactive oxygen species in the pathogenesis of early diabetic nephropathy. *J Diabetes Investig* 2015;**6**:137−9.
57. de Zeeuw D, Akizawa T, Audhya P, Bakris GL, Chin M, Christ-Schmidt H, et al. Bardoxolone methyl in type 2 diabetes and stage 4 chronic kidney disease. *N Engl J Med* 2013;**369**:2492−503.
58. Miyamoto S, Zhang G, Hall D, Oates PJ, Maity S, Madesh M, et al. Restoring mitochondrial superoxide levels with elamipretide (MTP-131) protects *db/db* mice against progression of diabetic kidney disease. *J Biol Chem* 2020;**295**:7249−60.
59. Van Buren PN, Toto R. Hypertension in diabetic nephropathy: epidemiology, mechanisms, and management. *Adv Chronic Kidney Dis* 2011;**18**:28−41.
60. Karg MV, Bosch A, Kannenkeril D, Striepe K, Ott C, Schneider MP, et al. SGLT-2-inhibition with dapagliflozin reduces tissue sodium content: a randomised controlled trial. *Cardiovasc Diabetol* 2018;**17**:5.
61. He B, Wang Z, Chen L, Zhou Z, Abliz Z. A rapid, sensitive, and selective liquid chromatography-mass spectrometry method for simultaneous quantification of astragaloside IV and cycloastragenol in mouse plasma and its application to a pharmacokinetic study. *Int J Mass Spectrom* 2018;**434**:130−5.
62. Sun H, Wang W, Han P, Shao M, Song G, Du H, et al. Astragaloside IV ameliorates renal injury in *db/db* mice. *Sci Rep* 2016;**6**:32545.
63. Liu X, Wang W, Song G, Wei X, Zeng Y, Han P, et al. Astragaloside IV ameliorates diabetic nephropathy by modulating the mitochondrial quality control network. *PLoS One* 2017;**12**:e0182558.
64. Wu H, Gao Y, Shi HL, Qin LY, Huang F, Lan YY, et al. Astragaloside IV improves lipid metabolism in obese mice by alleviation of leptin resistance and regulation of thermogenic network. *Sci Rep* 2016;**6**:30190.